Time-energy densities in $\pi \rightarrow \mu$ decay

B. Autin* and F. Méot†

*CERN AB, Geneva
†CEA DAPNIA, Saclay

Abstract. An analytical model is developed to describe the longitudinal phase space of a hybrid beam of pions and decay muons.

INTRODUCTION

The properties of the muon beam created by decay of pions are usually obtained by simulation. Here, an analytical model is developed to get insight into the properties of the beam and guidelines in the adjustment of the magnets of the decay channel and of the RF system that collect the muon beam. It is assumed that there is no coupling between transverse and longitudinal spaces. This treatment is thus more appropriate in the present stage for a quadrupolar than for a solenoidal decay channel. All the pions are supposed to travel along the axis of the channel. It is thus essentially the kinematic effects of the pion motion, muon creation and muon motion that are investigated. These effects are described in terms of energy or momentum density, of time density and of longitudinal phase space portraits. Densities are manipulated using random variable methods.

MOMENTUM AND ENERGY SPECTRA

Calculations that follow are based on the kinematical relations of the decay process $\pi \rightarrow \mu + \nu$. The following notations are used : pion mass m_π, its lifetime at rest τ_π^*, energy E_π, muon mass m_μ, center of mass decay angle θ_μ^* with respect to pion velocity. The basic kinematics ingredients needed are the pion

- laboratory frame lifetime $\tau_\pi = \gamma_\pi \tau_\pi^*$,
- decay law $N(s) = N_0 e^{-\eta s/p_\pi}$, wherein $\eta = m_\pi \ / \ c\tau_\pi^*$,

and the muon

- center of mass energy $E_\mu^* = (m_\pi^2 + m_\mu^2)/2m_\pi$ and momentum $p_\mu^* = (m_\pi^2 - m_\mu^2)/2m_\pi$,
- laboratory frame energy $E_\mu = \gamma_\pi(E_\mu^* + \beta_\pi p_\mu^* \cos\theta_\mu^*)$,

The technique used to calculate a density in some variable x as a function of a density in another variable y relies on the relation $g_x = g_y \ |dy/dx|$.

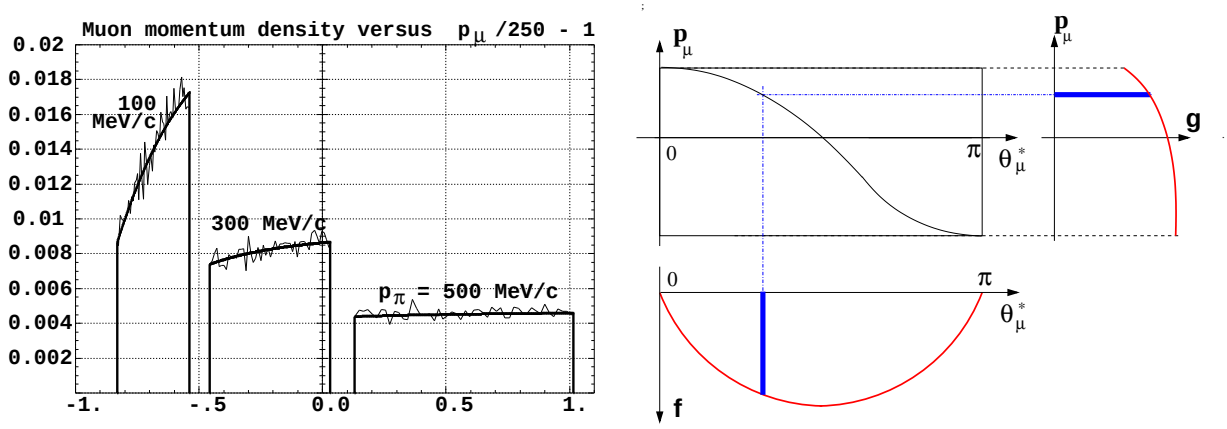

FIGURE 1. Density $g_{p_\mu|p_\pi}(p_\mu)$ for $p_\pi = 100,\ 300$ and 500 MeV/c (left graph), and geometrical understanding of its build-up from $g_{\theta^*}(\theta^*_\mu)$ in the change of variable $\theta^*_\mu \to p_\mu$ (right).

Muon spectra at fixed pion momentum

Muon momentum. Given fixed pion momentum p_π, the decay muon momentum satisfies a p_π-conditional density that writes

$$g_{p_\mu|p_\pi}(p_\mu) = g_{\theta^*}(\theta^*_\mu)\ \left|d\theta^*_\mu/dp_\mu\right| \tag{1}$$
$$= \frac{m_\pi}{2p_\pi p^*_\mu}\frac{p_\mu}{\sqrt{p^2_\mu+m^2_\mu}} = \frac{m_\pi}{2p_\pi p^*_\mu}\beta_\mu\ , \qquad p_\mu \in [\gamma_\pi(\beta_\pi E^*_\mu - p^*_\mu), \gamma_\pi(\beta_\pi E^*_\mu + p^*_\mu)]$$

wherein $g_{\theta^*}(\theta^*_\mu) = \sin\theta^*_\mu/2\ \ (\theta^*_\mu \in [0,\pi])$ is the decay angle density. $g_{p_\mu|p_\pi}(p_\mu) \equiv 0$ outside the specified p_μ interval. FIG. 1 shows typical shapes of $g_{p_\mu|p_\pi}(p_\mu)$. Monte Carlo histograms $\Delta N_{p_\mu|p_\pi}/N_0\Delta p_\mu$ are superimposed for comparison.

Muon energy. Similar calculations in the case of a change of variable $\theta^*_\mu \to E_\mu$, or as well using $d/dE = (1/\beta)d/dp$ in Eq. 1, yield the energy density at fixed p_π

$$g_{E_\mu|p_\pi}(E_\mu) = \frac{m_\pi}{2p_\pi p^*_\mu}\ , \qquad E_\mu \in [\gamma_\pi(E^*_\mu - \beta_\pi p^*_\mu), \gamma_\pi(E^*_\mu + \beta_\pi p^*_\mu)] \tag{2}$$

Pion and muon spectra versus flight distance

Pions. Pion densities properties that intervene in the sequel are as follows. The decay density as a function of flight distance s, given p_π, writes

$$g_{s|p_\pi}(s,p_\pi) = (\eta/p_\pi)\exp(-\eta s/p_\pi) \tag{3}$$

Given parent pions with initial momentum density $g_{p_\pi}(p_\pi)$ (say, at $s = 0$), one gets the 2-D density at arbitrary $s > 0$

$$g_{s,p_\pi}(s,p_\pi) = g_{s|p_\pi} \times g_{p_\pi} \qquad (\text{and } \int_{s=0}^{\infty}\int g_{s,p_\pi}(s,p_\pi)\,ds\,dp_\pi = 1) \tag{4}$$

In the following, for the sake of simplification, we will illustrate things using a uniform initial pion momentum density

$$g_{p_\pi}(p_\pi) = \mathbf{1}_{\Delta p_\pi}(p_\pi) = 1/(p_{\pi_2} - p_{\pi_1}) \qquad (p_\pi \in [p_{\pi_1}, p_{\pi_2}]) \tag{5}$$

The ensuing form of $g_{s,p_\pi}(s,p_\pi)$ is shown in FIG. 2, given a pion bunch launched at $s = 0$ with zero size and $p_\pi \in [100, 500]$ MeV/c. Integrating Eq. 4 with respect to s yields the p_π-density of the decayed parent pions at distance s,

$$g_{p_\pi}(p_\pi)\big|_s = \int_0^s g_{s,p_\pi}(s,p_\pi)\,ds = \mathbf{1}_{\Delta p_\pi}(p_\pi)\,(1 - \exp(-\eta s/p_\pi)) \tag{6}$$

The p_π-density of the *non-decayed* pion population ensues,

$$\bar{g}_{p_\pi}(p_\pi)\big|_s = (g_{p_\pi}(p_\pi) - g_{p_\pi}(p_\pi)\big|_s) = \mathbf{1}_{\Delta p_\pi}(p_\pi)\,\exp(-\eta s/p_\pi) \tag{7}$$

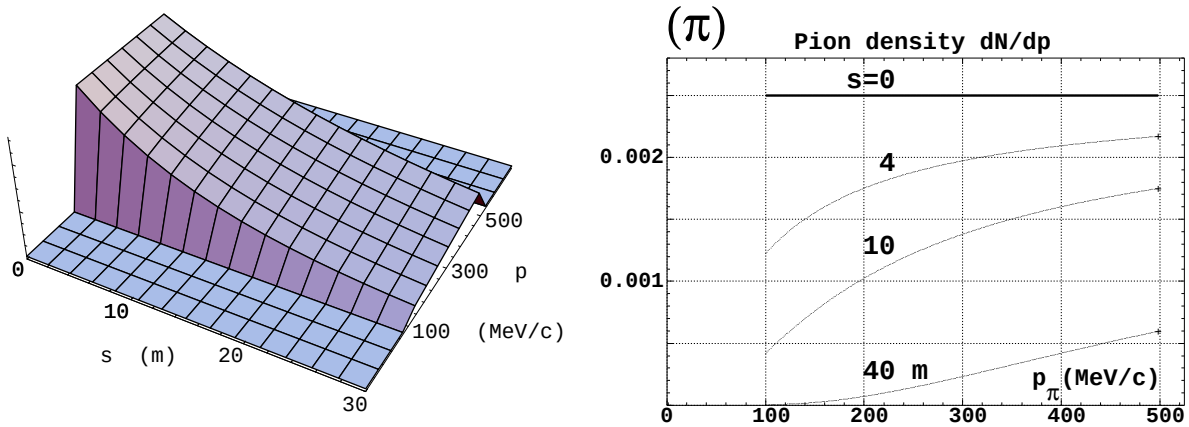

FIGURE 2. Pion momentum density along the decay channel (left graph) and s-sections (right).

Muons. A non-zero pion momentum byte is accounted for by multiplying the p_π-conditional density $g_{p_\mu|p_\pi}(p_\mu)$ (Eq. 1) by the muon density at s at given p_π, $g_{s,p_\pi}(s,p_\pi)$ (Eq. 4). (The muon decay is not taken into account in the following for simplicity, doing so would mean accounting for an s-dependent muon survival additional factor.) This yields the muon momentum spectrum at s under the integral form

$$g_{p_\mu}(p_\mu)|_s = \int_{\Delta p_\pi} g_{p_\mu|p_\pi}\,dp_\pi \int_0^s g_{s,p_\pi}(s,p_\pi)\,ds \qquad (\text{and } \lim_{s\to\infty} g_{p_\mu}(p_\mu)|_s = 1) \tag{8}$$

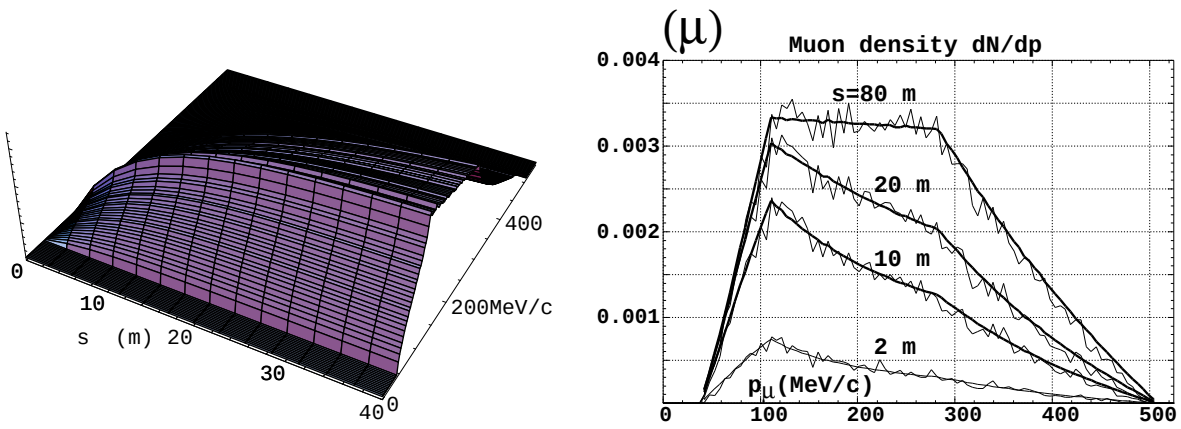

FIGURE 3. *Left :* muon momentum density along the decay channel. *Right : s*-sections.

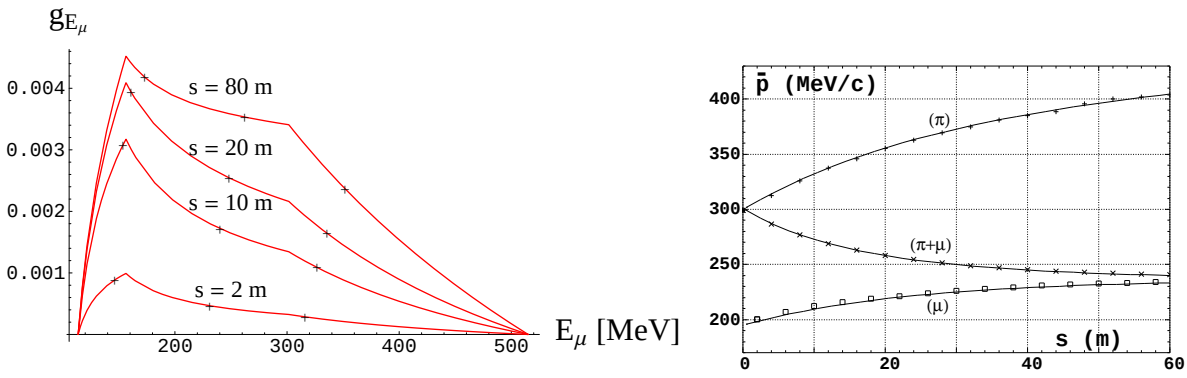

FIGURE 4. *Left :* Muon energy density at various distances s ; the crosses are at $\overline{E}_\mu$ and at $\overline{E}_\mu \pm \sigma_{E_\mu}$. *Right :* Average momentum of beams over 60 m flight distance (markers are from Monte Carlo simulations).

The Δp_π integration interval is a function of p_μ following the dependence given in Eq. 1 (not all pions can produce a muon of momentum p_μ). A similar integral holds for the energy spectrum $g_{E_\mu}(E_\mu)|_s$, given $g_{E_\mu|p_\pi}$ (Eq. 2).

The summation in Eq. 8 can be viewed as a superposition of the fixed-p_π muon spectra of FIG. 1, this is the way the muon spectra shown in FIG. 3 has been numerically calculated (Monte Carlo histograms $\Delta N_{p_\mu}|_s / N_0 \Delta p_\mu$ have been superimposed for comparison). However the calculations can been completed analytically, as performed for obtaining the energy spectra in FIG. 4-left, which we do not detail for shortness.

Mean value and standard deviation

Parent pion beam. The pion beam average momentum as a function of s is obtained from Eq. 7 that yields

$$\overline{p}_\pi(s) = \int p\ \overline{g}_{p_\pi}(p)|_s\, dp \;/\; \int \overline{g}_{p_\pi}(p)|_s\, dp = \frac{\sum_{i=1,2}(-)^i \frac{p_{\pi_i}^2 - \eta\, s\, p_{\pi_i} - \eta^2 s^2 e^{\frac{\eta s}{p_{\pi_i}}}\, \mathrm{Ei}(-\frac{\eta s}{p_{\pi_i}})}{2e^{\eta s/p_{\pi_i}}}}{\sum_{i=1,2}(-)^i \frac{p_{\pi_i} + \eta\, s e^{\frac{\eta s}{p_{\pi_i}}}\, \mathrm{Ei}(-\frac{\eta s}{p_{\pi_i}})}{e^{\eta s/p_{\pi_i}}}}$$

Muon beam. Similar calculations apply to the determination of the mean momentum $\overline{p}_\mu(s)$ and energy $\overline{E}_\mu(s)$ of the muons and to the momentum of the center of gravity of the hybrid beam.

Average momenta of both pion and muon beams are increasing functions of the distance, because the lower energy parent pions decay faster, whereas the average momentum of the $\pi + \mu$ beam decreases monotonically here (FIG. 4-right), a behavior that can be accounted for to maintain constant focusing strength in tuning the decay channel [1].

Another parameter, relevant to the voltage of the RF system, is the second moment of the energy density:

$$\sigma_{E_\mu}(l) = \Big(\int_{E_{\mu 1}}^{E_{\mu 2}} (E - \overline{E}_\mu)^2 g_{E_\mu}\, dE \;\Big/\; \int_{E_{\mu 1}}^{E_{\mu 2}} g_{E_\mu}\, dE \Big)^{1/2} \tag{9}$$

Both mean energy and ends of the standard energy interval are displayed in FIG. 4-right . The capture efficiency can be defined as

$$y_{E_\mu}(s) \;=\; \int_{\overline{E}_\mu - \sigma_{E_\mu}}^{\overline{E}_\mu + \sigma_{E_\mu}} g_{E_\mu}\, dE \;\Big/\; \int_{E_{\mu 1}}^{E_{\mu 2}} g_{E_\mu}\, dE \tag{10}$$

TIME SPECTRA

The approach followed for the energy distribution can be resumed for time distribution. The p_π-conditional time density $g_{t_\mu|p_\pi}(p_\mu)$ of the muons at arbitrary s can be derived from $g_{\theta^*}(\theta_\mu^*)$ through a change of variable

$$\theta_\mu^* \;\rightarrow\; t_\mu = s_d/c\beta_\pi \;+\; (s - s_d)/c\beta_\mu$$

On the other hand $g_{t_\mu|p_\pi}(p_\mu)$ can be derived from $g_{p_\mu|p_\pi}(p_\mu)$ (Eq. 1) using a change of variable $p_\mu \rightarrow t_\mu$.

A non-zero pion momentum byte Δp_π is accounted for in the muon density calculation, by introducing the decayed pion density at s_d, under the form of a $g_{s,p_\pi}(s, p_\pi)$ factor (Eq. 4). This yields the muon time density under the integral form

$$g_{t_\mu}(t_\mu)|_s = \int_{s_d=0}^{s} ds_d \int_{\Delta p_\pi} g_{t_\mu|p_\pi}(t_\mu)\, g_{s,p_\pi}(s_d, p_\pi)\, dp_\pi \tag{11}$$

with still a p_μ dependence, and in addition a s_d dependence, of the integration domain Δp_π. The calculation cannot be performed analytically because of the presence of β_π together with p_π in the integrand. Moreover, integrating over s cannot be done separately.

The numerical method of histograms superimposition followed for calculating the momentum and energy densities remains however valid. The boundary times correspond to the fastest and slowest muon emitted by the fastest and slowest pion. The typical shape of $g_{t_\mu}(t_\mu)|_s$ is displayed as a projected density in FIG. 6. The first two moments of $g_{t_\mu}(t_\mu)|_s$ can be calculated so as to derive capture efficiencies as was done for the energy spectra.

Proton bunch length. The time distribution is affected by the length τ of the proton bunch which generates the pions by interaction with the target (which in turn affects the muon yield [2,Tab. 5.2]). This is a matter of re-writing the density function under the form of a convolution product $g_{t_\mu}(t_\mu)|_s = \frac{1}{\tau}\int_0^\tau S(t_\mu-\tau)g_{t_\mu}(\tau)|_s \; d\tau$, wherein S characterizes the density of pions inside the bunch at the time of production.

LONGITUDINAL PHASE-SPACE

The muon time density $g_{t_\mu}(t_\mu)|_s$ (Eq. 11) has an explicit dependence on s. Note that, given the pion energies in concern here, the flight distance s can be considered in good approximation as the position along the channel length. $g_{t_\mu}(t_\mu)|_s$ also has an implicit

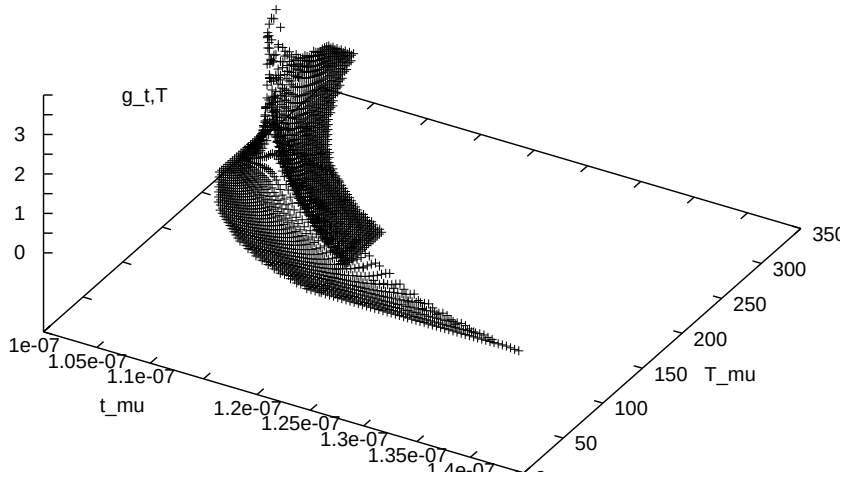

FIGURE 5. Muon density (in arbitrary units) at $s = 30$ m, in a time-Kinetic energy frame.

dependence on p_μ or E_μ (from the $p_\mu \leftrightarrow t_\mu$ correlation). As a consequence $g_{t_\mu}(t_\mu)|_s$ can be considered as a 2-D density $g_{t_\mu,E_\mu}(t_\mu,E_\mu)|_s$ in the longitudinal phase-space with parameter s. This is illustrated in FIG. 5 in the case $p_\pi \in [200,400]$ MeV/c and $s = 30$ m.

The muon population at arbitrary s can also be reconstructed from Eq. 11 : the (t_μ,E_μ) space can be meshed, $N_0 g_{t_\mu,E_\mu}(t_\mu,E_\mu)|_s \Delta p_\mu \Delta E_\mu$ gives the local number of points on the mesh. This is illustrated in FIG. 6-left, taking $p_\pi \in [200,400]$ MeV/c and $s = 40$ m. Monte Carlo simulations of longitudinal phase-space at distance s along a drift axis are

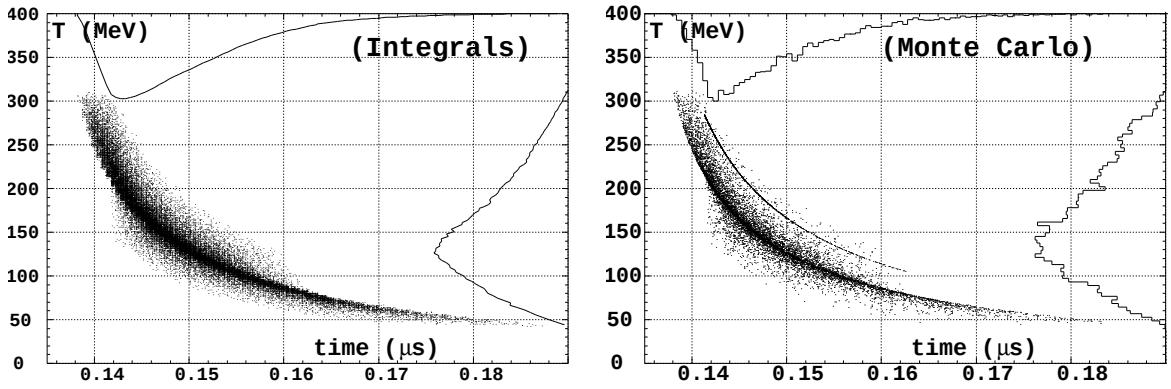

FIGURE 6. Muon longitudinal phase-space (time-Kinetic energy) at $s = 40$ m (the thin arc on the right plot is the survived pion bunch).

displayed in Fig. 6-right for comparison, showing excellent agreement, in particular it is seen that time and energy projected densities superimpose fairly well.

RF parameters

The first two moments of the marginal densities g_{t_μ} and g_{E_μ} can be calculated as described earlier, in the conditions illustrated in FIG. 5, which yields the following results. The bunch distribution in time and in energy satisfy

$$\overline{ct}_\mu \pm \sigma_{ct_\mu} = 33.5 \pm 1.6 \text{ m}, \qquad \overline{E}_\mu \pm \sigma_{E_\mu} = 258 \pm 55 \text{ MeV}$$

The *rms* time extent determines the choice of 45 MHz RF frequency for a half-wave extent, whereas σ_{E_μ} determines a ≈ 55 MV total RF voltage, for bunch rotation (consistent with the CERN design parameters [2,Sec.5.2]).

The *rms* bunch emittance is $\varepsilon/\pi = 1.23$ eV.s, yielding a

capture efficiency of 64%

namely, the ratio of the number of muons contained in the *rms* bunch to the total number of muons. The ct_μ to E_μ correlation coefficient is -0.87. The proton bunch length upper limit in order to avoid excessive muon bunch lengthening is about 5 ns (in quadratic mean).

CONCLUSION

The model described in this paper explains the shape of the density functions of a muon beam and allows calculating the 2-D longitudinal phase-space density. The calculations can be applied to a realistic pion spectrum once HARP will have provided its results [3], yet the hypothesis of uniform spectrum is fairly well fulfilled for a $\pi^\pm$ momentum

interval of $150 - 500$ MeV/c [4], allowing an estimate of various parameters entering muon capture dynamics.

The energy and time densities can be given an simple integral form and thus calculated numerically almost instantaneously. Moreover several of the integral expressions involved have an analytical primitive, this has not been detailed for the sake of shortness.

Various quantities relevant to beam dynamics can be derived : average beam momentum applies to the adjustment of the focusing strength of the quadrupoles in the decay channel. The mean energy and the energy spread affect the RF voltage. The mean arrival time and the muon bunch length are relevant to the RF phase and the choice of the RF frequency. The predictions of the model have been compared with results from Monte Carlo simulations for validation.

Calculation and transport of the *transverse* densities and phase-space portraits have been undertaken in a similar way [5], and will be subject to further publication.

Further developments and applications can be foreseen, including fast propagation of densities by methods of second order transport, using techniques of random variables and their combination.

Acknowledgments

We thank A. Verdier (CERN) for fruitful discussions, O. Napoly (CEA) for pointing out an error on $g_{\theta^*}(\theta_\mu^*)$ in an earlier stage of the work and J. Doornbos (TRIUMF) for Monte Carlo cross checks using GEANT.

References

1. B. Autin, F. Lemuet, F. Méot, A. Verdier, Optimization Of A Quadrupole Funnel/Decay Channel, these proceedings, and
B. Autin, F. Méot, A. Verdier, Efficiency Of An Alternating Gradient Muon Collection Channel, CERN NUFACT Note 128 (2003)
2. Study Of A European Neutrino Factory Complex, CERN NUFACT Note 122 (2002)
3. Expected for July 2004, cf. A. Tonazzo, "Status of HARP", Muon week 17-19 Nov. 2003, CERN, http://muonstoragerings.web.cern.ch/muonstoragerings/Events/200311
4. B. Autin, Technical challenges of neutrino factories, NIM A Vol. 451, Issue 1, 21 Aug. 2000, Pages 244-254, and
Johann Collot, Harold G. Kirk and Nikolai V. Mokhov, Pion production models and neutrino factories, *ibidem*, Pages 327-330
5. F. Méot, Proc. FFAG03 workshop, KEK, Tsukuba (July 2003)